Chemistry–A European Journal

Research Article
doi.org/10.1002/chem.202404632

Chemistry Europe
European Chemical Societies Publishing

www.chemeurj.org

Synthesis and Chiroptical Activity of π-Expanded Electron-Rich Heterohelicenes Based on the 1,4-Dihydropyrrolo[3,2-*b*]pyrrole Core

Damian Kusy,[a] Krzysztof Górski,[a] Francesco Bertocchi,[b] Matteo Galli,[b] Nicolas Vanthuyne,[c] Francesca Terenziani,*[b] and Daniel T. Gryko*[a]

Herein, we report the synthesis and chiroptical characteristics of the first (double) helicenes possessing the 1,4-dihydropyrrolo[3,2-*b*]pyrrole (DHPP) moiety as their central core. We have developed a three-step synthesis with 6π-electrocyclization accompanied by HBr elimination as its key step. We found that, whereas for smaller peripheral arms double 6π-electrocyclization occurs smoothly forming a double helicene, in the case of longer polycyclic aromatic hydrocarbons the reaction becomes less efficient and mono-helicenes are the only products. The electron density distribution analysis of LUMO explains the different regioselectivity of 6π-electrocyclization. The synthesized heterohelicenes are characterized by greenish-blue emission, distinct solvatofluorochromism and good fluorescence quantum yields (up to 42%). Moreover, the chiroptical measurements reveal that unsymmetrical double heterohelicene exhibits excellent circularly polarized luminescence brightness (B_{CPL}) reaching 30 $M^{-1}cm^{-1}$. The combined experimental and computational study has revealed that a charge-transfer state is responsible for the observed emission (hence the solvatochromism), while low-energy absorption derives from multiple transitions.

Introduction

Heterohelicenes belong to the class of *ortho*-fused aromatics containing at least one heteroatom incorporated into the helix backbone (Figure 1).[1] One of the factors drawing the attention of scientists towards these compounds is their unique molecular 3D architecture, which makes them an ideal scaffold to be used in complex stereodynamics studies.[2–5] Their chirality allows for effective implementation as auxiliaries in asymmetric synthesis.[6] Proper functionalization of the helical structure leads to two-photon absorbers[7] and "turn-on" fluorescence sensing materials.[8,9] Moreover, some helicenes can be effectively applied in cell imaging[10] and recent reports also shed light on the bioactivity of these molecules, leading them to be used as selective drugs in treating renal cell carcinoma.[11] It should also be mentioned that helicenes, like other aromatic systems, find applications in optoelectronics, e.g. organic light emitting devices (OLED),[12–14] organic field effect transistors (OFET)[15] and organic photovoltaics (OPV).[16,17] Many recent studies have been devoted to chirality-induced spin selectivity (CISS).[18]

The most dynamically developing applications in the field of helicenes, however, are technologies directly utilizing their chiroptical activity, e.g. circular dichroism (CD)[19] and circularly polarized luminescence (CPL).[20] Relatively small helicenes

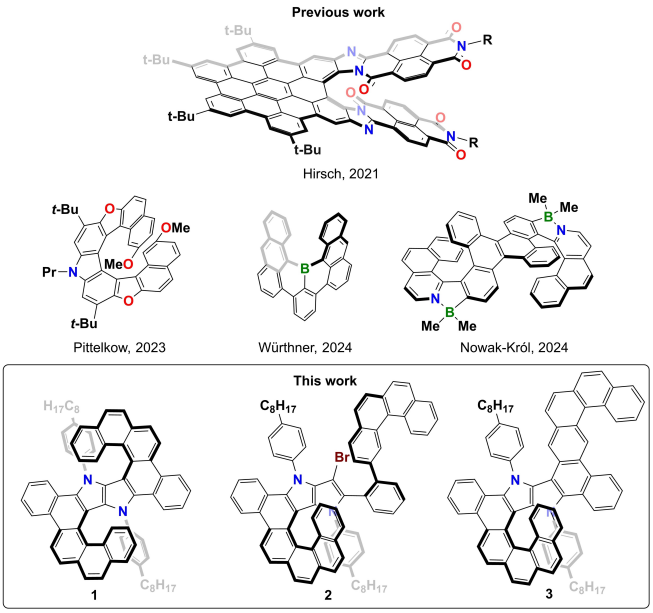

Figure 1. Chemical structures of representative π-expanded heterohelicenes.

[a] D. Kusy, K. Górski, D. T. Gryko
Institute of Organic Chemistry, Polish Academy of Sciences, Kasprzaka 44–52, 01-224 Warsaw, Poland
E-mail: dtgryko@icho.edu.pl

[b] F. Bertocchi, M. Galli, F. Terenziani
Department of Chemistry, Life Sciences and Environmental Sustainability, University of Parma, 43124 Parma, Italy
E-mail: francesca.terenziani@unipr.it

[c] N. Vanthuyne
Aix Marseille Univ, CNRS, Centrale Marseille, UAR 1739, FSCM, Chiropole, Marseille, France

Supporting information for this article is available on the WWW under https://doi.org/10.1002/chem.202404632

exhibit rather low fluorescence quantum yields (Φ_{FL}) and their absorption dissymmetry factor (g_{abs}) as well as luminescence dissymmetry factor (g_{lum}) are both in the range of 10^{-4}–10^{-2}, leaving much space for improvement.[21,22] Indeed the appropriate design of heterohelicenes enhances fluorescence quantum yield and chiroptical responses.[23–33] For instance, the peripheral decoration of the helicene scaffold *via* naphthalimide subunits, results in a rise of Φ_{FL} from 4% up to 70%.[34] Likewise, it was shown that heteroatom doping or distinct π-electron system expansion increases the dissymmetry factors.[35–37] Furthermore, appropriate molecular design governs long-lived circular polarization of phosphorescence.[38,39] In most reported cases of heterohelicenes, the aromatic heterocycle is present at the periphery. We became interested in exploring if a heterocyclic scaffold possessing quadrupolar symmetry can play the role of the central core in double heterohelicenes. We have chosen 1,4-dihydropyrrolo[3,2-*b*]pyrrole (DHPP)[40,41] as the central core because of the following combination of properties: (1) Straightforward synthesis *via* multicomponent reaction which is resistant to steric hindrance present in substrates' structure; (2) Formation of a densely substituted scaffold which at the same time is amenable to facile functionalization; (3) Strong emission intensity almost regardless of structural modifications.[42] In addition the exceptionally electron-rich character of DHPP core can have a potential to introduce mild polarization of the double helicene which according to earlier reports can have beneficial effect for luminescence dissymmetry factor.[43,44] We present here a readily accessible synthetic protocol towards π-expanded, electron-rich double heterohelicenes, exhibiting fluorescence in the visible range with good quantum yields.

Design and Synthesis

Our idea was to build double helical structures by assembling two helicenes at the periphery of the DHPP core (**1**, Figure 1). We designed two double helicenes differing in length i.e. a [6]helicene and a [7]helicene, respectively. We envisioned that our recently developed strategy based on 6π-electrocyclization accompanied by HBr elimination,[45] would be the best tool to build two helical units. The universality of this strategy is based on the ability of tetraarylpyrrolo[3,2-*b*]pyrrole (TAPP) to be brominated at positions 3 and 6, which shortens the synthetic approach and enhances its efficiency. The synthesis of compound **1** started from the Suzuki-Miyaura coupling reaction of 3-bromophenanthrene and (2-formylphenyl)boronic acid using $Pd(PPh_3)_4$ as the catalyst, which afforded 2-(phenanthren-3-yl)benzaldehyde **4** in an excellent yield of 80% (see ESI for details). The next step was a multicomponent reaction between aldehyde **4**, 4-*n*-octylaniline and butane-2,3-dione, catalyzed by iron(III) perchlorate, which gave TAPP **5** in 70% yield. Intermediate **5** was brominated using N-bromosuccinimide, smoothly leading to **6** in 77% yield (Scheme 1). In the last key step, compound **6** was subjected to 6π-electrocyclization, which allowed us to obtain the desired double helicene **1** in 10% yield. Regrettably, debrominated TAPPs and intractable polar substances constitute the remaining products. The same sequence of reactions was used to attempt the synthesis of double [7]helicene starting from benzophenanthrene instead of phenanthrene. In the first stage we used 2-bromobenzo[*c*]phenanthrene obtained according to the procedure of Jakubec *et al.*[46]

The next steps were the synthesis of TAPP **8** followed by a bromination reaction to obtain **9** (Scheme 2). In contrast to the previous case, 6π-electrocyclization of dye **9** did not afford a double [7]helicene, but afforded instead helicenes **2** and **3** in low yields (Scheme 2). The latter is the unexpected product of a double 6π-electrocyclization. The course of 6π-electrocyclization of TAPP **9** can be explained *via* analysis of electron density distribution at the LUMO level of **2**. Firstly, the symmetry of the wave function within the 6π-electrocyclization center indicates that, upon excitation, the bonding interaction between the helical arm and the DHPP core can be achieved, leading to **3** (Figure 2, dark red). Secondly, a clear bonding character of the orbital, between [4]helicene and benzene ring as well as benzene ring and DHPP subunit, are stabilizing the presented conformation (Figure 2). These two factors are directly responsible for the observed regiospecificity of the photocyclization process. On the other hand, the steric hindrance induced by the [4]helicene moiety, as well as the relatively small electron density within the 6π-electrocyclization center (orbital contour value = 0.008), makes the discussed interaction not efficient, which stands in line with a small reaction yield of **3** (4%). Moreover, the photocyclization time leading to **3** was elongated

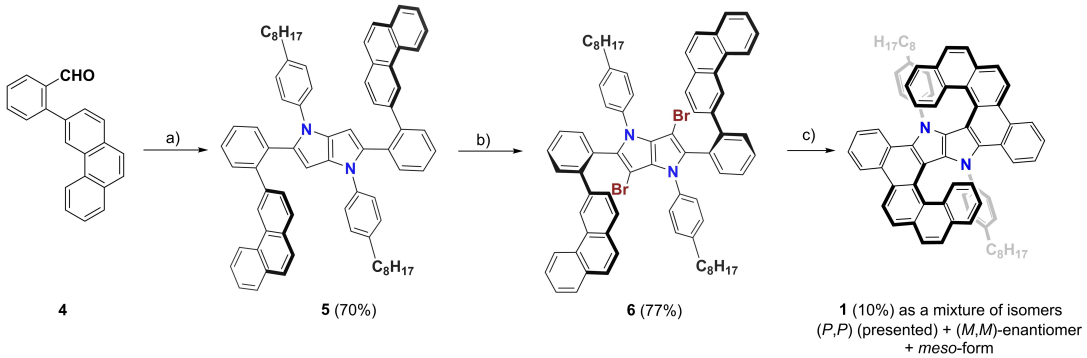

4 **5** (70%) **6** (77%) **1** (10%) as a mixture of isomers (*P*,*P*) (presented) + (*M*,*M*)-enantiomer + *meso*-form

Scheme 1. Synthetic route to compound **1**. Reagents and conditions: a) 4-*n*-octylaniline, butan-2,3-dione, $Fe(ClO_4)_3$ xH_2O (6 mol%), AcOH/toluene, 50 °C, 16 h, b) $CHCl_3$, NBS (N-Bromosuccinimide), c) UV, DIPEA, hexane 3 h.

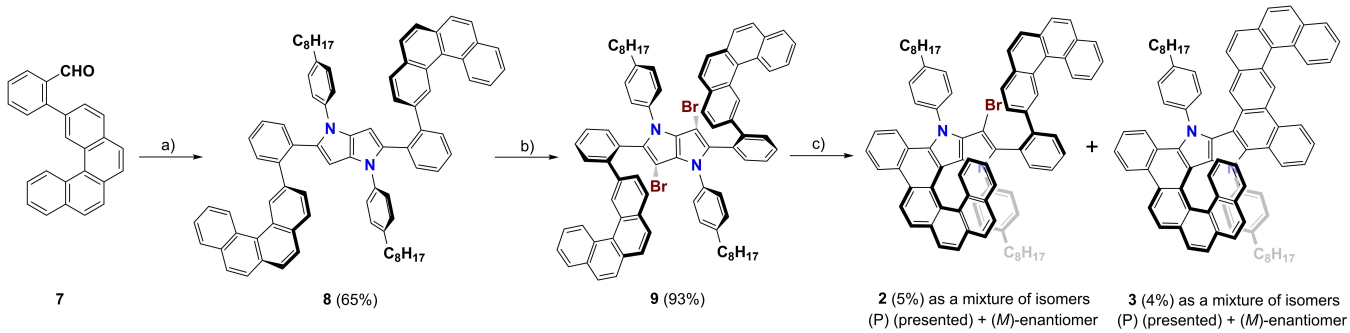

Scheme 2. Synthetic route to compound **2**, **3**. Reagents and conditions: a) 4-*n*-octylaniline, butan-2,3-dione, $Fe(ClO_4)_3$ H_2O (6 mol%), AcOH/toluene, 50 °C, 16 h, b) $CHCl_3$, NBS (N-Bromosuccinimide), c) UV, DIPEA, hexane 32 h.

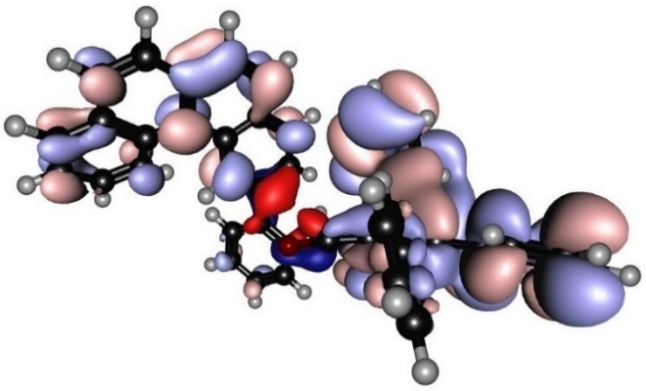

Figure 2. LUMO of 2 for contour value 0.008, dark red and dark blue represent electron density involved in the 6π-electrocyclization process.

up to 32 h, more than 10 times longer in comparison to **1**, for which the electrocyclization process takes place in around 3 h.

The structures of **1** and **3** were verified by variable-temperature nuclear magnetic resonance (NMR) analysis and high-resolution mass spectra. For these molecules, owing to the rotation of the p-*n*-octyl benzene rings, we observed coalescence of the peaks of the protons of the 4-*n*-octylbenzene rings at room temperature, while at low temperature (233 K) we observed four peaks (Figures S15, and S20, Supporting Information). These results indicate that the observed behavior of the 4-n-octylbenzene substituents is due torsion of the aryl group.[47,48] All compounds **1**–**3** showed high photostability under ambient light in air at room temperature, as well as good solubility in various solvents such as methylene chloride (DCM), toluene and dimethyl sulfoxide (DMSO). The final three compounds (**1**–**3**) were obtained as a racemic mixture along with, in the case of dye **1**, the meso-form. The meso-form was not obtained in a pure state after chiral HPLC separation. The enantiomers, comprising 60% of the initial mixture subjected to separation, were recovered in an equimolar ratio (1:1). These compounds were separated into their enantiomers using chiral HPLC. For each compound, both enantiomers were successfully isolated with an enantiomeric excess (ee) of 99.5% (the enantiomeric excesses were determined by chiral HPLC). Additional details can be found in the supporting information.

Photophysical Properties

Helicenes **1**–**3** photophysical properties were investigated experimentally and *via* computational analysis. Depending on the degree of annulation, the obtained helicenes can be divided into two groups: fully fused (helicenes **1** and **3**) and semi-fused (helicene **2**). Due to the semi-fused structure, dye **2** possesses the largest energy gap between frontiers orbitals, $\Delta E = 3.42$ eV (Figure 4). On the other hand, annulation results in distinct destabilization of HOMO level, up to −4.64 eV and −4.61 eV, and stabilization of LUMO to −1.44 eV and −1.43 eV, for **1** and **3**, respectively. Interestingly, the presence of two additional benzene rings in **3** compared to **1**, as well as different molecular structure and symmetry, only slightly affects the energy of frontier orbitals, thus the HOMO-LUMO gap barely changes (Figure 4).

Absorption and fluorescence spectra of the investigated compounds are reported in Figure 3. Despite the differences in molecular architecture, helicenes **1**–**3** share some common spectroscopic features, e.g. weak to moderate absorption of visible light below 500 nm, and strong absorption in the violet spectral region and in the UV region (Figure 3, Table 1). The computational analysis shows that the electron density at HOMO, as well as HOMO-1, is mostly localized on the electron-rich DHPP core and partially on the helical arm (Figure 4). On the other hand, LUMO of **1** is primarily placed at the molecule's center, while in the case of **2** and **3**, it is distinctly shifted to one of the helical arms. A similar displacement of the electron density toward the molecular periphery is observed for the LUMO + 1 level of all the investigated systems. TDDFT calculations indicate that, for all systems, HOMO→LUMO is the main contribution to the $S_0 \rightarrow S_1$ transition. It is worth mentioning that the contribution of HOMO→LUMO + 1 cannot be omitted for dye **3** (Table S1). The electron density separation between occupied (HOMO) and unoccupied orbitals (LUMO, LUMO + 1) involved in the first electronic transition leads to relatively small oscillator strengths, explaining the weak absorption in most parts of the visible region. The observed experimental molar absorption coefficients (ε) are $\approx 2500\ M^{-1}cm^{-1}$ (@ 437 nm), $\approx 3000\ M^{-1}cm^{-1}$ (@ 446 nm) and $\approx 10000\ M^{-1}cm^{-1}$ (@ 456 nm) for **1**, **2** and **3**, respectively (Table 1). TD-DFT results suggest that the longest-wavelength band in the experimental absorp-

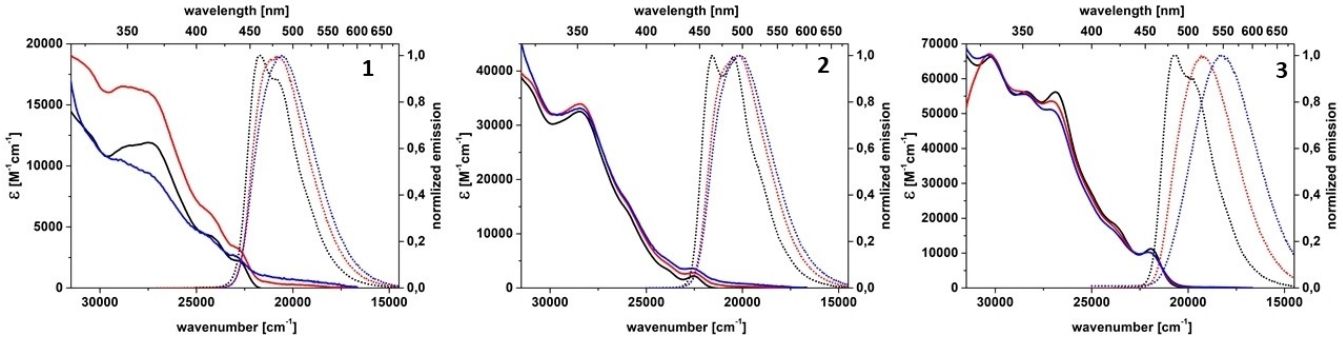

Figure 3. Absorption (solid lines) and emission spectra (dots) of **1**–**3** in toluene (black), dichloromethane (red) and dimethyl sulfoxide (blue).

Table 1. Spectroscopic data in toluene, dichloromethane and dimethyl sulfoxide for helicenes **1**–**3**.

Helicene	Solvent	λ_{abs} [nm] ($\varepsilon \cdot 10^{-3}$ [cm^{-1} M^{-1}])	λ_{em} [nm]	$\Delta\nu$ [cm^{-1}]	Φ_{FL} [%]	τ [ns]	$k_r \cdot 10^{-7}$ [s^{-1}]	$k_{nr} \cdot 10^{-7}$ [s^{-1}]
1	Tol	350 (11.6), 364 (11.9), 410 (4.4), 438 (2.2)	460, 481	1100	27.0	4.32	6.3	17
	DCM	350 (16.5), 364 (16.0), 412 (6.1), 437 (3.3)	481	2100	25.0	4.63	5.4	16
	DMSO	350 (10.1), 364 (9.4), 407 (4.4), 435 (2.6)	486	2400	29.4	–	–	–
2	Tol	350 (32.5), 446 (2.1)	463, 488	800	4.5	1.80	2.5	53
	DCM	350 (33.9), 446 (2.9)	495	2200	3.3	1.72	1.9	56
	DMSO	350 (33.1), 446 (3.5)	495	2200	3.1	–	–	–
3	Tol	330 (66.2), 350 (56.2), 372 (56.2), 456 (11.2)	483, 505	1200	32.4	4.62	7.0	15
	DCM	330 (66.2), 350 (56.2), 369 (53.6), 456 (10.0)	520	2700	25.6	6.68	3.8	11
	DMSO	330 (66.2), 350 (56.2), 369 (51.1), 456 (10.0)	546	3600	42.5	–	–	–

$\lambda_{abs}/\lambda_{em}$ – absorption/emission wavelength, ε – molar absorption coefficient, Φ_{FL} – fluorescence quantum yield, $\Delta\nu$ – Stokes shift, τ – fluorescence lifetime, k_r/k_{nr} – radiative/nonradiative decay constants.

tion spectra is actually due to the superposition of many peaks near each other ($S_0 \rightarrow S_{1\text{-}7}$). Strong absorption in the violet and UV region is due to transitions in the range $S_0 \rightarrow S_{8\text{–}12}$.

In emission spectra of **1**–**3** in toluene, a clear vibronic progression is observed. However, upon increasing solvent polarity, the vibronic structure is smeared out by inhomogeneous broadening (Figure 3). This is consistent with emission from a charge-transfer state, in agreement with the differences in electron density distribution over HOMO and LUMO (Figure 4). Further confirmation is given by the dipole moment of the lowest-energy excited state (S_1), amounting to 0.7, 8.5 and 11.2 D, for **1**, **2** and **3**, respectively (relaxed excited state), while the ground state has smaller dipole moment (0.0, 1.2 and 1.1 D, respectively). The charge-transfer nature of the S_1 state is particularly pronounced for **3**, causing a noticeable solvatofluorochromism[49–51] (the emission wavelength moves from 483 nm in toluene to 546 nm in dimethyl sulfoxide, Figure 3, Table 1).

Analysis of radiative and nonradiative decay constants (k_r and k_{nr}) gives more insight into the nature of the emitting excited state. For helicenes **1** and **2**, k_r and k_{nr} values are slightly affected by solvent polarity, thus fluorescence quantum yields (Φ_{FL}) are also barely affected (Table 1). It resembles the previously described butterfly-shaped π-expanded pyrrolopyrroles.[52] In analogy to those dyes, the lack of dependence of Φ_{FL} on increasing solvent polarity can be attributed to the presence of excited states that are close in energy but have different polarization directions. The nonradiative decay constant of helicene **2** is more than three times larger than for helicenes **1** or **3**. This observation is directly associated with the bromine atom presence, which enhances spin-orbit coupling. As a result of effective nonradiative deactivation of the S_1 state through intersystem crossing,[53] the fluorescence quantum yield of **2** is nearly ten times smaller compared to **1** or **3** (Table 1). Increased solvent polarity distinctly affects the nature of the S_1 state for **3**, as shown by a nearly two-fold drop in the radiative constant when passing from toluene to dichloromethane.

Chiroptical Properties

CD spectra of the pairs of enantiomers of **1**, **2** and **3** in DCM (Figure 5, full lines) show multiple peaks, with dissymmetry factors, g_{abs}, lower than 10^{-2} (see Figure S21). The longest-wavelength peak in the CD spectra (located at 449, 446 and 457 nm for **1**, **2** and **3**, respectively) is very weak for **1**, while its intensity becomes two and seven times higher for **2** and **3**, respectively. For **1**, the CD spectrum in the region of the longest-wavelength peak is enlarged in the inset of the left panel. Since the longest-wavelength transition is related to the Kasha state, we expect the g_{abs} value related to that transition to be very similar to the $|g_{lum}|$ value relevant to CPL.[54,55] CPL spectra (reported in Figure 5, as thin lines with dots) correspond well in position and shape to the corresponding fluorescence spectra. The luminescence dissymmetry factors of the enantiomers of each pair are in good agreement, with $|g_{lum}|$ on the

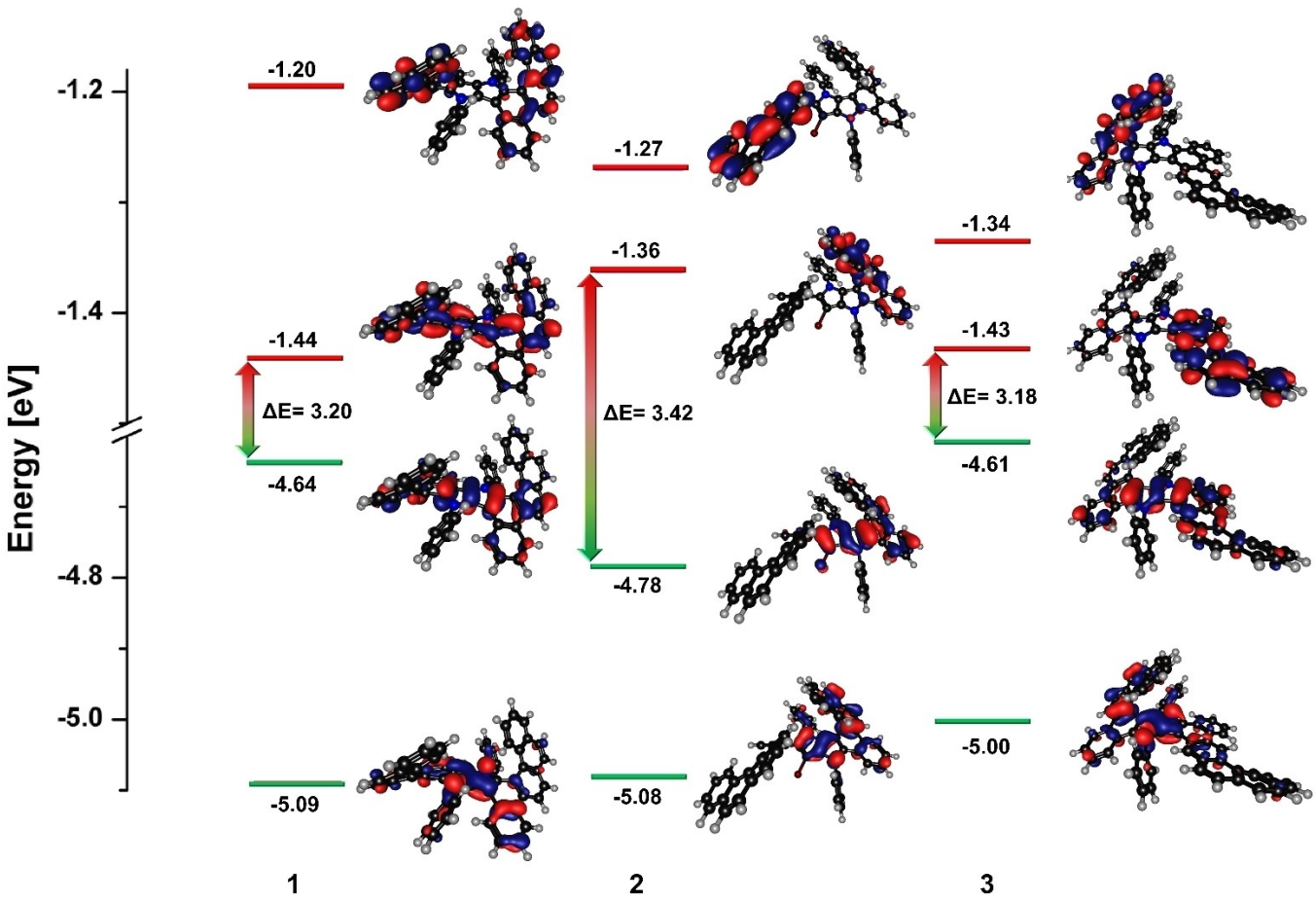

Figure 4. Energy diagram for helicenes **1**–**3**. Results obtained from DFT B3LYP calculations. Occupied orbitals (green), unoccupied orbitals (red). Orbital contour value = 0.03.

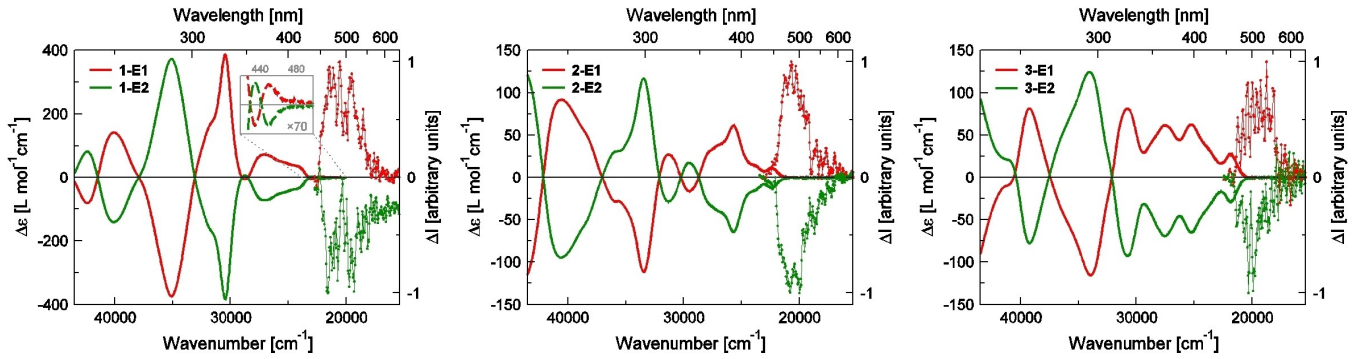

Figure 5. CD (full lines) and CPL (thin lines with dots) spectra of the enantiomers of **1**, **2** and **3** in DCM. The inset in the left panel shows the enlargement of the longest-wavelength Cotton effect for the two enantiomers of compound **1**.

order of 10^{-3} for **1** and **3**, and approaching 10^{-2} for **2**, in both solvents. The $|g_{lum}|$ values are very similar to the g_{abs} values relevant to the lowest-energy CD bands, suggesting that minimal geometrical rearrangements take place in the excited state prior to emission. As anticipated by the CD spectra, **1** has the lowest $|g_{lum}|$ factor. In general, we observe that higher radiative decay constants (typically associated with high luminescence quantum yields, Table 1) correspond to lower $|g_{lum}|$ values, since it can be shown that $g_{lum} \propto 1/\sqrt{k_r}$.[56] To take into account the overall CPL performance of a sample, in addition to its dissymmetry factor, the CPL brightness (B_{CPL}) was introduced.[57] The values of B_{CPL} for our compounds are reported in Table 2, showing that the enantiomers of compound **3** have the highest CPL brightness, comparable with other S-shaped helicenes reported in the literature.[57–63]

In order to assign the right absolute configuration to each eluted fraction of **1**–**3**, we performed TD-DFT calculations following the described procedure,[64] just skipping the molec-

Table 2. Helicene-based emitters **1**–**3** and their g_{lum}, fluorescence quantum yield, absorption coefficient at 350 nm ($M^{-1}cm^{-1}$), and CPL brightness ($M^{-1}cm^{-1}$). Solvent: toluene – first line, methylene chloride – second line.

	g_{lum} (E1/E2)	Φ_{FL}	ε [$M^{-1}\cdot cm^{-1}$] @ 350 nm	B_{CPL}
1	$+1.20\times10^{-3}/-1.33\times10^{-3}$	27%	11600	2.0
	$+1.89\times10^{-3}/-1.95\times10^{-3}$	25%	16500	4.0
2	$+5.60\times10^{-3}/-6.11\times10^{-3}$	4.5%	32500	4.3
	$+6.64\times10^{-3}/-7.22\times10^{-3}$	3.3%	33900	3.9
3	$+3.20\times10^{-3}/-3.25\times10^{-3}$	32.4%	56200	29.3
	$+2.60\times10^{-3}/-2.33\times10^{-3}$	25.6%	56200	17.7

ular dynamics simulations sampling, thanks to the high structural rigidity of the chiral chromophoric cores which limits the conformational degrees of freedom. The comparison of the calculated and experimental CD spectra (mainly the sign of the different peaks) allowed to assign the absolute configuration. The comparison is reported in Figure S23 and shows good agreement in the spectral shape and energies for both absorption and CD of **1**–**3**. In general, enantiomers showing a positive rotational strength for the lowest energy CD peak were found to be P (or P, P in the case of **1**) helixes.

The sign of the lowest-energy CD peak of the calculated spectrum stands in line with the experimental one for **2** and **3**, while for **1** the calculated sign was the opposite. This inconsistency does not surprise, since **1** has an extremely low rotational strength relative to the Kasha state, therefore even tiny geometry variations can alter its sign. In particular, the sign is highly sensitive to the precise orientation of the phenyl groups linked to the pyrrolo[3,2-b]pyrrole nitrogens, which are spatially close to the two helixes. Moreover, the right sign of the lowest energy CD peak is recovered if the phenyl groups are substituted with methyl groups, the rest of the CD spectrum staying practically unaffected.

Conclusions

It is possible to synthesize double [6]helicene in just three steps from aromatic aldehydes and primary aromatic amines *via* a sequence starting from multicomponent reaction leading to the formation of 1,4-dihydropyrrolo[3,2-*b*]pyrrole core followed by bromination and 6π-electrocyclization accompanied by the HBr elimination. The size of the peripheral arm influences the reaction output: in the case of more sterically encumbered scaffolds, 6π-electrocyclization occurs in a different way. Out of three structurally diverse helicenes, [7]helicene **3** turned out to be the best performing one for several reasons: it shows a large molar extinction coefficient in the violet spectral region, it has an impressive fluorescence quantum yield of 32% and a high circularly polarized luminescence brightness (B_{CPL}) of $\approx30\ M^{-1}cm^{-1}$. Interestingly, the $|g_{lum}|$ factor for helicene **2** possessing one benzophenanthrene moiety perpendicularly bridged with helicene reaches 7.22×10^{-3} which stands it out from the chiral optical activity of known helicenes. This research impacts the development of advanced OLEDs and fluorescence imaging technologies. Further exploration of longer helicenes and multihelicenes with controlled optoelectronic properties is crucial for continued progress in these fields.

Experimental Section

General. All reagents and solvents were purchased from commercial sources and were used as received unless otherwise noted. For water-sensitive reactions, solvents were dried using the Solvent Purification System from MBraun (https://www.mbraun.com/us/). Reactions involving moisture and oxygen-sensitive compounds were performed under a stream of argon. The reaction progress was monitored by means of thin layer chromatography (TLC), which was performed on aluminium foil plates, covered with Silica gel 60 F254 (Merck). Products' purification was done by means of column chromatography with Kieselgel 60 (200–400 mesh, Merck). The identity and purity of prepared compounds were proved by ^{1}H NMR and ^{13}C NMR spectrometry as well as by MS-spectrometry (via EI-MS, ESI-MS or APCI-MS). NMR spectra were measured on Bruker AM 500 MHz, Varian 600 MHz, Varian 500 MHz instruments with TMS as internal standard. Chemical shifts for ^{1}H NMR are expressed in parts per million (ppm) relative to tetramethylsilane (δ 0.00 ppm), $CDCl_3$ (δ 7.26 ppm) CD_2Cl_2 (δ 5.33 ppm). Chemical shifts for ^{13}C NMR are expressed in ppm relative to $CDCl_3$ (δ 77.16 ppm), CD_2Cl_2 (53.84 ppm). Data are reported as follows: chemical shift, multiplicity (s = singlet, bs = broad singlet, d = doublet, dd = doublet of doublets, ddd = doublet of doublet of doublets, t = triplet, td = triplet of doublets, q = quartet, qu = quintet, m = multiplet), coupling constant (Hz), and integration.

Photophysical properties. UV-Vis absorption spectra were recorded in toluene, dichloromethane and DMSO in 1 cm quartz cuvettes at room temperature using dilute solutions ($C\approx10^{-6}$ M) in order to avoid additional bands from aggregates and fluorescence reabsorption in emission spectra. Emission spectra were obtained upon excitation at 350 nm (slits = 1) for **1**–**3**. To determine the fluorescence quantum yield in solution, quinine sulphate solution in 0.5 M H_2SO_4 ($\Phi = 0.51$) was used as a standard.

Computational details. Gaussian 16 suite was used for calculations.[65] Each structure was optimized to a minimum for the ground state at a DFT level of theory, using B3LYP as functional and 6–31G(d) as the basis set, in the gas phase (optimized geometries are reported in Figure S23). TD-DFT calculations were performed on the optimized structure using three different functionals (B3LYP, CAM–B3LYP, M062X), showing good stability of the results. In all the calculations, the octyl chains have been replaced by methyl groups, to reduce the number of structures with similar energies, speed up the calculations and obtain more reliable results. Absorption and CD spectra were calculated using 30 excited states, assigning to each of them a Gaussian bandshape of appropriate bandwidth (typically around 0.1 eV).

Acknowledgements

This work has received funding from the European Union's Horizon2020 research and innovation programme under the Marie Skłodowska-Curie grant agreements No 101007804 (Micro4Nano) and No 860762. The work was financially supported by the Polish National Science Centre, Poland (OPUS 2020/37/B/ST4/00017) and has benefited from the equipment and framework of the COMP-HUB and COMP-R initiatives, funded by the "Departments of Excellence" program of the

Italian Ministry for University and Research (MIUR, 2018-2022 and MUR, 2023-2027).

Conflict of Interests

The authors declare no conflict of interest.

Data Availability Statement

The data that support the findings of this study are available in the supplementary material of this article.

Keywords: Helicene · Dyes/pigments · Pyrrole · Fluorescence · Circularly polarized luminescence

[1] D. Volland, J. Niedens, P. T. Geppert, M. J. Wildervanck, F. Full, A. Nowak-Król, *Angew. Chem. Int. Ed.* **2023**, *62*, e202304291.
[2] C. Li, Y. Yang, Q. Miao, *Chem. Asian J.* **2018**, *13*, 884–894.
[3] W. Yang, J. Shen, *Chem. Eur. J.* **2022**, *28*, e202202069.
[4] Y. Wu, S. Ying, S. Liao, L. Zhang, J. Du, B. Chen, H. Tian, F. Xie, H. Xu, S. Deng, Q. Zhang, S. Xie, L. Zheng, *Angew. Chem. Int. Ed.* **2022**, *61*, e202204334.
[5] M. Akiyama, K. Nozaki, *Angew. Chem. Int. Ed.* **2017**, *56*, 2040–2044.
[6] P. Aillard, A. Voituriez, A. Marinetti, *Dalt. Trans.* **2014**, *43*, 15263–15278.
[7] Z. Hu, L. Li, Z. Liu, Z. Liu, D. Zhang, K. Li, *ChemPlusChem* **2020**, *85*, 742–750.
[8] M. Hasan, V. N. Khose, T. Mori, V. Borovkov, A. V. Karnik, *ACS Omega* **2017**, *2*, 592–598.
[9] A. Petdum, W. Panchan, P. Swanglap, J. Sirirak, T. Sooksimuang, N. Wanichacheva, *Sens. Actuators, B* **2018**, *259*, 862–870.
[10] M. Li, L.-H. Feng, H.-Y. Lu, S. Wang, C.-F. Chen, *Adv. Funct. Mater.* **2014**, *24*, 4405–4412.
[11] X. He, F. Gan, Y. Zhou, Y. Zhang, P. Zhao, B. Zhao, Q. Tang, L. Ye, J. Bu, J. Mei, L. Du, H. Dai, H. Qiu, P. Liu, *Small Methods* **2021**, *5*, 2100770.
[12] S. Jhulki, A. K. Mishra, T. J. Chow, J. N. Moorthy, *Chem. Eur. J.* **2016**, *22*, 9375–9386.
[13] K. Yavari, W. Delaunay, N. De Rycke, T. Reynaldo, P. Aillard, M. Srebro-Hooper, V. Y. Chang, G. Muller, D. Tondelier, B. Geffroy, A. Voituriez, A. Marinetti, M. Hissler, J. Crassous, *Chem. Eur. J.* **2019**, *25*, 5303–5310.
[14] K. Dhbaibi, L. Favereau, M. Srebro-Hooper, M. Jean, N. Vanthuyne, F. Zinna, B. Jamoussi, L. Di Bari, J. Autschbach, J. Crassous, *Chem. Sci.* **2018**, *9*, 735–742.
[15] Y. Yang, R. C. da Costa, M. J. Fuchter, A. J. Campbell, *Nat. Photonics* **2013**, *7*, 634–638.
[16] P. Josse, L. Favereau, C. Shen, S. Dabos-Seignon, P. Blanchard, C. Cabanetos, J. Crassous, *Chem. Eur. J.* **2017**, *23*, 6277–6281.
[17] J. Wang, H. Shi, N. Xu, J. Zhang, Y. Yuan, M. Lei, L. Wang, P. Wang, *Adv. Funct. Mater.* **2020**, *30*, 2002114.
[18] R. Naaman, D. H. Waldeck, *J. Phys. Chem. Lett.* **2012**, *3*, 2178–2187.
[19] N. Berova, L. Di Bari, G. Pescitelli, *Chem. Soc. Rev.* **2007**, *36*, 914.
[20] J. Han, S. Guo, H. Lu, S. Liu, Q. Zhao, W. Huang, *Adv. Opt. Mater.* **2018**, *6*, 1800538.
[21] T. Mori, *Chem. Rev.* **2021**, *121*, 2373–2412.
[22] M. Schnitzlein, K. Shoyama, F. Würthner, *Chem. Sci.* **2024**, *15*, 2984–2989.
[23] A. Nowak-Król, P. T. Geppert, K. R. Naveen, *Chem. Sci.* **2024**, *15*, 7408–7440.
[24] F. Full, A. Artigas, K. Wiegand, D. Volland, K. Szkodzinska, Y. Coquerel, A. Nowak-Krol, *J. Am. Chem. Soc.* **2024**, *146*, 29245–29254.
[25] M. Schnitzlein, K. Shoyama, F. Würthner, *Chem. Sci.* **2024**, *15*, 2984–2989.
[26] F. Saal, F. Zhang, M. Holzapfel, M. Stolte, E. Michail, M. Moos, A. Schmiedel, A. M. Krause, C. Lambert, F. Würthner, P. Ravat, *J. Am. Chem. Soc.* **2020**, *142*, 21298–21303.
[27] C. Dusold, D. I. Sharapa, F. Hampel, A. Hirsch, *Chem. Eur. J.* **2021**, *27*, 2332–2341.
[28] S. S. Warthegau, A. E. Hillers-Bendtsen, S. K. Pedersen, C. Rindom, C. Bræstrup, J. S. Jensen, O. Hammerich, M. S. Thomsen, F. S. Kamounah, P. Norman, K. V. Mikkelsen, T. Brock-Nannestad, M. Pittelkow, *Chem. Eur. J.* **2023**, *29*, e202301815.
[29] D. Tan, J. Dong, T. Ma, Q. Feng, S. Wang, D. T. Yang, *Angew. Chem. Int. Ed.* **2023**, *62*, e.202304711.
[30] T. Katayama, S. Nakatsuka, H. Hirai, N. Yasuda, J. Kumar, T. Kawai, T. Hatakeyama, *J. Am. Chem. Soc.* **2016**, *138*, 5210–5213.
[31] X. Y. Wang, X. C. Wang, A. Narita, M. Wagner, X. Y. Cao, X. Feng, K. Müllen, *J. Am. Chem. Soc.* **2016**, *138*, 12783–12786.
[32] F. Aribot, A. Merle, P. Dechambenoit, H. Bock, A. Artigas, N. Vanthuyne, Y. Carissan, D. Hagebaum-Reignier, Y. Coquerel, F. Durola, *Angew. Chem. Int. Ed.* **2023**, *62*, e202304058.
[33] A. Artigas, F. Rigoulet, M. Giorgi, D. Hagebaum-Reignier, Y. Carissan, Y. Coquerel, *J. Am. Chem. Soc.* **2023**, *145*, 15084–15087.
[34] X. Tian, K. Shoyama, B. Mahlmeister, F. Brust, M. Stolte, F. Würthner, *J. Am. Chem. Soc.* **2023**, *145*, 9886–9894.
[35] Y. Shen, N. Yao, L. Diao, Y. Yang, X. Chen, H. Gong, *Angew. Chem. Int. Ed.* **2023**, *62*, e.202300840.
[36] J.-K. Li, X.-Y. Chen, Y.-L. Guo, X.-C. Wang, A. C.-H. Sue, X.-Y. Cao, X.-Y. Wang, *J. Am. Chem. Soc.* **2021**, *143*, 17958–17963.
[37] G. R. Kiel, H. M. Bergman, A. E. Samkian, N. J. Schuster, R. C. Handford, A. J. Rothenberger, R. Gomez-Bombarelli, C. Nuckolls, T. D. Tilley, *J. Am. Chem. Soc.* **2022**, *144*, 23421–23427.
[38] E. S. Gauthier, L. Abella, N. Hellou, B. Darquié, E. Caytan, T. Roisnel, N. Vanthuyne, L. Favereau, M. Srebro-Hooper, J. A. G. Williams, J. Autschbach, J. Crassous, *Angew. Chem. Int. Ed.* **2020**, *59*, 8394–8400.
[39] L. Norel, M. Rudolph, N. Vanthuyne, J. A. G. Williams, C. Lescop, C. Roussel, J. Autschbach, J. Crassous, R. Réau, *Angew. Chem.* **2010**, *122*, 103–106.
[40] A. Janiga, E. Glodkowska-Mrowka, T. Stoklosa, D. T. Gryko, *Asian J. Org. Chem.* **2013**, *2*, 411–415.
[41] M. Krzeszewski, D. Gryko, D. T. Gryko, *Acc. Chem. Res.* **2017**, *50*, 2334–2345.
[42] G. Sanil, B. Koszarna, Y. M. Poronik, O. Vakuliuk, B. Szymański, D. Kusy, D. T. Gryko, *Adv. Heterocycl. Chem.* **2022**, *138*, 335–409.
[43] K. Dhbaibi, L. Abella, S. Meunier-Della-Gatta, T. Roisnel, N. Vanthuyne, B. Jamoussi, G. Pieters, B. Racine, E. Quesnel, J. Autschbach, J. Crassous, L. Favereau, *Chem. Sci.* **2021**, *12*, 5522–5533.
[44] H. Kubo, T. Hirose, T. Nakashima, T. Kawai, J. Hasegawa, K. Matsuda, *J. Phys. Chem. Lett.* **2021**, *12*, 686–695.
[45] K. Górski, L. Pejov, K. B. Jørgensen, I. Knysh, D. Jacquemin, D. T. Gryko, *Chem. Eur. J.* **2025**, *31*, e202404094.
[46] M. Jakubec, T. Beránek, P. Jakubík, J. Sýkora, J. Žádný, V. Církva, J. Storch, *J. Org. Chem.* **2018**, *83*, 3607–3616.
[47] Y. Yu, L. Wang, C. Wang, F. Liu, H. Ling, J. Liu, *Small Sci.* **2024**, *4*, 2400176.
[48] J. Malinčík, S. Gaikwad, J. P. Mora-Fuentes, M. A. Boillat, A. Prescimone, D. Häussinger, A. G. Campaña, T. Šolomek, *Angew. Chem. Int. Ed.* **2022**, *61*, e202208591.
[49] R. Dhali, D. K. A. Phan Huu, F. Bertocchi, C. Sissa, F. Terenziani, A. Painelli, *Phys. Chem. Chem. Phys.* **2021**, *23*, 378–387.
[50] A. Marini, A. Muñoz-Losa, A. Biancardi, B. Mennucci, *J. Phys. Chem. B* **2010**, *114*, 17128–17135.
[51] B. Boldrini, E. Cavalli, A. Painelli, F. Terenziani, *J. Phys. Chem. A* **2002**, *106*, 6286–6294.
[52] B. Bardi, M. Krzeszewski, D. T. Gryko, A. Painelli, F. Terenziani, *Chem. Eur. J.* **2019**, *25*, 13930–13938.
[53] M. Mac, A. Danel, K. Kizior, P. Nowak, A. Karocki, B. Tokarczyk, *Phys. Chem. Chem. Phys.* **2003**, *5*, 988–997.
[54] F. S. Richardson, J. P. Riehl, *Chem. Rev.* **1977**, *77*, 773–792.
[55] J. P. Riehl, F. S. Richardson, *Chem. Rev.* **1986**, *86*, 1–16.
[56] J. L. Greenfield, J. Wade, J. R. Brandt, X. Shi, T. J. Penfold, M. J. Fuchter, *Chem. Sci.* **2021**, *12*, 8589–8602.
[57] L. Arrico, L. Di Bari, F. Zinna, *Chem. Eur. J.* **2021**, *27*, 2920–2934.
[58] S. Kinoshita, R. Yamano, Y. Shibata, Y. Tanaka, K. Hanada, T. Matsumoto, K. Miyamoto, A. Muranaka, M. Uchiyama, K. Tanaka, *Angew. Chem. Int. Ed.* **2020**, *59*, 11020–11027.
[59] Y. Kimura, Y. Shibata, K. Noguchi, K. Tanaka, *Eur. J. Org. Chem.* **2019**, *2019*, 1390–1396.
[60] Q. Jiang, Y. Han, Y. Zou, H. Phan, L. Yuan, T. S. Herng, J. Ding, C. Chi, *Chem. Eur. J.* **2020**, *26*, 15613–15622.
[61] J. M. dos Santos, D. Sun, J. M. Moreno-Naranjo, D. Hall, F. Zinna, S. T. J. Ryan, W. Shi, T. Matulaitis, D. B. Cordes, A. M. Z. Slawin, D. Beljonne, S. L.

Warriner, Y. Olivier, M. J. Fuchter, E. Zysman-Colman, *J. Mater. Chem. C* **2022**, *10*, 4861–4870.
[62] T. Kawashima, Y. Matsumoto, T. Sato, Y. M. A. Yamada, C. Kono, A. Tsurusaki, K. Kamikawa, *Chem. Eur. J.* **2020**, *26*, 13170–13176.
[63] A. V. Gulevskaya, E. A. Shvydkova, D. I. Tonkoglazova, *Eur. J. Org. Chem.* **2018**, *2018*, 5030–5043.
[64] G. Pescitelli, T. Bruhn, *Chirality* **2016**, *28*, 466–474.
[65] M. J. Frisch, G. W. Trucks, H. B. Schlegel, G. E. Scuseria, M. A. Robb, J. R. Cheeseman, G. Scalmani, V. Barone, G. A. Petersson, H. Nakatsuji, X. Li, M. Caricato, A. V. Marenich, J. Bloino, B. G. Janesko, R. Gomperts, B. Mennucci, H. P. Hratchian, J. V. Ortiz, A. F. Izmaylov, J. L. Sonnenberg, D. Williams-Young, F. Ding, F. Lipparini, F. Egidi, J. Goings, B. Peng, A. Petrone, T. Henderson, D. Ranasinghe, V. G. Zakrzewski, J. Gao, N. Rega, G. Zheng, W. Liang, M. Hada, M. Ehara, K. Toyota, R. Fukuda, J. Hasegawa, M. Ishida, T. Nakajima, Y. Honda, O. Kitao, H. Nakai, T. Vreven, K. Throssell, J. A. Montgomery Jr., J. E. Peralta, F. Ogliaro, M. J. Bearpark, J. J. Heyd, E. N. Brothers, K. N. Kudin, V. N. Staroverov, T. A. Keith, R. Kobayashi, J. Normand, K. Raghavachari, A. P. Rendell, J. C. Burant, S. S. Iyengar, J. Tomasi, M. Cossi, J. M. Millam, M. Klene, C. Adamo, R. Cammi, J. W. Ochterski, R. L. Martin, K. Morokuma, O. Farkas, J. B. Foresman, D. J. Fox, *Gaussian 16, Revision C.01*, Gaussian, Inc., Wallingford, CT **2016**.

Manuscript received: December 16, 2024
Accepted manuscript online: January 22, 2025
Version of record online: February 5, 2025